

pubs.acs.org/Macromolecules Article

Electrophoretic Translocation of Star-Shaped Polymers through Single Solid-State Nanopores

Kuo Chen, Minglun Li, and Murugappan Muthukumar*



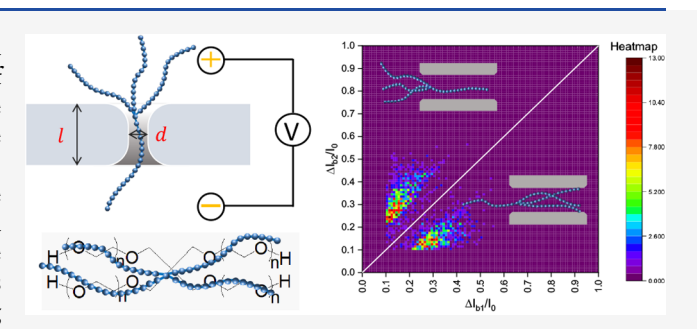
Cite This: Macromolecules 2024, 57, 6693-6704



ACCESS I

Metrics & More

ABSTRACT: While the translocation of linear polymers through nanopores is well-understood, the underlying mechanism of transport of branched polymers through nanopores is yet to be fully developed. In this general premise, we have investigated the translocation of multiarm star-like polyethylene glycols (PEGs) through single solid-state nanopores, using single-molecule electrophoresis. Our experiments reveal the conformational trajectories of multiarm-PEGs during their sojourn inside the nanopore in exquisite detail. We quantify these pathways in terms of the number of leading arms ($f_{\rm int}$), which depend on the pore diameter (d) and the total



Article Recommendations

number of arms (f). We have measured the average translocation time (τ) , polymer capture rate (R_c) , and polymer conformations during translocation in terms of d, f, and applied voltage (V_m) . We find a direct proportionality between R_c and f/V_m , and between τ and f/V_m . Interestingly, star polymers with more arms inside the nanopore (f_{in}) than outside (f_{out}) also translocate successfully, in contrast with previous suggestions of $f_{in} < f_{out}$. As the pore size increases, the optimal f_{in} shifts from 0.25f to 0.5f. In addition to gaining insight into the mechanism of translocation of star-like polymers, the present experimental strategy opens new opportunities to characterize and separate polymers with different branching architectures.

INTRODUCTION

Movement of macromolecules through narrow channels or membranes is a ubiquitous process in many natural situations with wide-ranging applications that span from biological material transfer among different spatial domains to industrial separation techniques. ¹⁻⁶ A molecular understanding of this transport process is essential for gaining insights into myriads of complex biological scenarios and optimizing separation protocols in industrial settings. During the past several decades, advances in nanopore technology have enabled indepth single-molecule investigations of both natural and synthetic polymer translocation through protein nanopores and solid-state nanopores. 7-37 Even though significant progress has been made in understanding the transport of linear charged macromolecules, less attention has been given to polymers with unique architectures, such as ring, star-shaped, branched, and bottle-brush polymers. ^{7-9,22,23,27-29,31,32} As a specific example, a star-polymer with f arms can adopt several different conformations during its translocation pathway, which in turn can result in different speeds. These possible conformations are illustrated in Figure 1 for f = 6. There are several different ways by which the molecule can traverse the pore. The number f_{in} of leading arms can, in principle, be any number from one to six. Since there are six chain ends, capture with $f_{in} = 6$ is favorable for larger pores. On the other hand, if the pore diameter is small enough, then all ends cannot be

captured due to entropic reasons and spatial limitations. Furthermore, when the arms are partitioned into $f_{\rm in}$ leading arms and $f_{\rm out}$ lagging arms, the frictional resistance against translocation can be complex. Hence, optimization of capture rate and translocation speed is cumbersome for developing strategies for the most efficient characterization and selectivity processes. Furthermore, the conformational trajectories of even one star-like polymer can adopt different pathways (Figure 1) and hence confuse the interpretation of their net measured speed. The primary goal of the present paper is to experimentally investigate several f-arm-star polymers toward a fundamental understanding of the mechanism of their translocation through a narrow nanopore.

Generally speaking, there have so far been two kinds of approaches to investigate the transport of star-like polymers. In one approach, a flow field is used to drive the star-polymer through a porous membrane or a matrix of multiple nanopores.^{22,23} In the other approach, which we use in the

Received: May 13, 2024 Revised: June 26, 2024 Accepted: July 1, 2024 Published: July 9, 2024





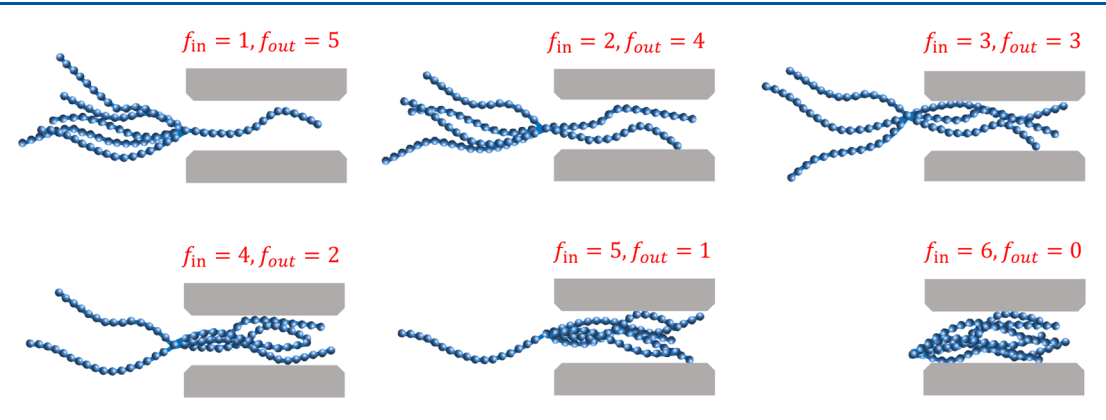


Figure 1. Sketch of different conformational partitioning of 6-arm-star polymer during its sojourn inside a nanopore.

present work, single star-polymers are driven through a single nanopore using an electric field. Accompanying these experiments, there have also been significant theoretical and simulation approaches. 7,27,28,33,34

In the context of flow-induced translocation, de Gennes⁷ predicted a critical flow rate (q_c) necessary for the translocation of star-shaped polymers through a nanopore of diameter d, by considering the entropic barrier associated with squeezing multiple arms into a nanopore. This rate follows a scaling relation of $q_c \sim f(d/na)^{2/3}$, where *n* denotes the number of repeated units on each arm and a represents the monomer size. An optimal number of forward arms (f_{in}) was suggested to be ranging from 1 to 0.5f. f_{in} represents the number of arms inside the nanopore when the polymer chain is captured by the nanopore. Experimental results in ultrafiltration of polystyrene stars demonstrated that q_c increases with f for a fixed n, while remaining independent of n for a given f_n observed across a range of R_h/d values from 2.2 to 6.1, where R_h is the hydrodynamic radius of the polymer in the absence of nanopore. Furthermore, the speculated f_{in} derived from the flow rate dependence on the relative retention of star chains was found to be 0.5f, and independent of n. This experimental finding is not consistent with the theoretical prediction. However, these results indicate that star-shaped polymers tend to pass through the nanopore with symmetric conformations. Subsequent simulations suggested that $f_{\rm in}$ could vary from 0.25f to 0.5f with an increase in $d.^{28}$

In the other context of electrophoretic translocation of starshaped polymers, there has so far been only one experimental investigation. This is based on star-shaped DNA molecules synthesized through DNA hybridization, 31,32 where the number of arms spans from 2 to 12, and the nanopore diameter ranges between 4 and 13 nm. The short doublestranded DNA branches are of 25 base pairs, so these arms act more like rigid rods than flexible chains due to their length being shorter than the persistence length of double-stranded DNA (approximately 150 base pairs). The analysis of the blockage current shape during translocation indicated that these star-shaped DNA chains primarily passed through the nanopore symmetrically, though some asymmetrical passages were noted in smaller pores. The semiflexible nature of doublestranded DNA led to distinct conductance blockages (ΔG) with a noticeable dependence on f, facilitating the characterization of mixtures with two or three components. Furthermore, star-shaped DNA exhibited higher capture rates and longer dwell times (τ) during translocation compared to linear counterparts. These results on dsDNA stars show that single-molecule electrophoresis technique can be successfully used to investigate the underlying translocation mechanism of other star-shaped polymers such as the ones studied in the present work.

In addition to the above-mentioned experimental work, there have been several simulation studies on the electrophoretic translocation of star-shaped polymers. Katkar and Muthukumar²⁹ used Langevin dynamics simulations to investigate the effects of f, d, and nanopore length (1) on τ , while keeping the total number of monomers (N) constant. They observed a nonmonotonic dependence of τ on f, identifying a critical value of f for the fastest translocation, which was found to be closely related to d. This phenomenon was attributed to the balance between the driving force inside the pore and the repulsive interactions between the arms as they enter the pore. Moreover, they discovered that translocation becomes unfeasible for a star-shaped polymer in a small pore when f exceeds a certain threshold value. These findings offer a method for characterizing and separating starshaped polymers through single-molecule electrophoresis techniques. Following this, Nagarajan and Chen³³ employed dissipative particle dynamics to explore the impact of varying solvent qualities on au and the temporal evolution of chain conformation during electrophoretic translocation. Extending the observation of a nonmonotonic relationship between au and f with a constant N, they also determined that the critical electric field strength necessary for translocation is dependent on both f and the length of the arms. This highlights the potential for using electrophoretic translocation through a nanopore to separate star-shaped polymers with different arm

Amidst the above-described current status on the translocation features of star-like polymers, we have studied the translocation of f-arm stars using single-molecule electrophoresis through a single nanopore, by keeping the length of the flexible chain arm fixed and varying f. By recognizing the discovery in the literature that the nominally neutral polyethylene glycol (PEG) behaves like a polycation in aqueous solutions containing KCl, and that it undergoes translocation through the α -hemolysin nanopore under electric fields, 11,14,17,24,38,39 we have chosen f-arm-PEGs (with f=2, 4, 6, and 8) as the star-polymers.

Briefly, the experimental procedure in the present investigation of single-molecule electrophoresis through a nanopore is the following. A nanopore separates a receiver compartment and a donor compartment (where the starpolymer is initially dispersed), and the ionic current in the

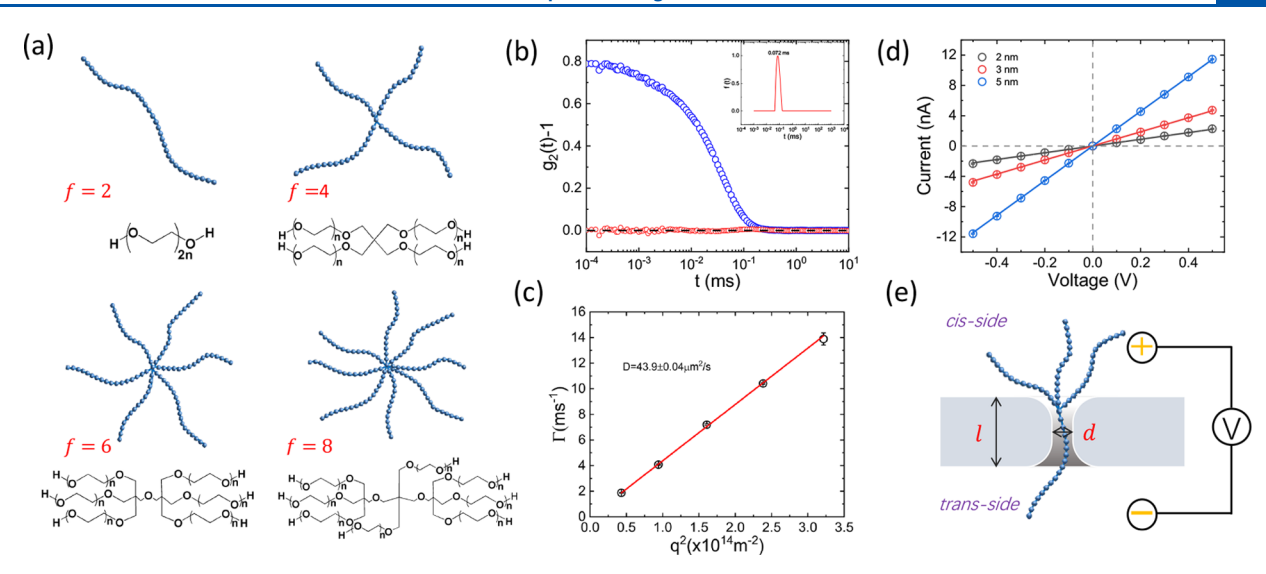


Figure 2. (a) Schematics of the chemical structures of multiarm-PEGs. (b) Intensity—intensity correlation function versus delay time at the scattering angle of 90° for 8-arm-PEG in 4 M KCl solution. The red curve denotes the residuals for the fitting of the experimental data in blue. (c) Quadratic dependence of the exponential decay rate of intensity—intensity correlation function, with the slope giving the diffusion coefficient D. (d) Current—voltage (I-V) curves of three solid-state nanopores with different diameters. Measurements were conducted in buffer solution containing 3.6 M LiCl, 10 mM HEPES at pH 8.0. (e) Illustration of the solid-state nanopore translocation setup, where d represents the diameter of the nanopore, and l is the thickness of the membrane chip, which is also considered as the length of the nanochannel.

assembly is measured. Whenever a single star-polymer is transported across the nanopore, the measured ionic current of the electrolyte solution shows a depression for a certain time duration. The signatures of such current blockages reveal exquisite details of the conformational modes of the transit of star-polymers through the nanopore. We have directly inferred conformational states of the *f*-arm-PEG during translocation through a well-defined single nanopore, which have so far been only discussed through theoretical and simulation approaches. In addition, we measure the dependencies of capture rate and average translocation time on the number of arms, pore diameter, and applied voltage and interpret the results.

The rest of the paper is organized as follows. The experimental setup and the materials are described in section 2. Section 3 provides details on the various characteristics of multiarm-PEG translocation that include translocation time, capture rate, conformational partitioning, and confinement effects. The final section summarizes the major findings and future perspective.

MATERIALS AND METHODS

Multiarm PEG Samples. Four multiarm PEGs of uniform arm length of degree of polymerization $n=113\ (5000\ \mathrm{g/mol})$ with number f of arms of 2, 4, 6, and 8, were purchased from JenKem (JenKem, USA) and used as received in the experiments. The chemical structure and their characteristics are given in Figure 2a and Table 1, respectively.

Table 1. f, $M_{\rm w}$, $R_{\rm h}$, and $R_{\rm h}/d$ of Multiarm PEGs in Solutions with 4 M KCl

code	f	$M_{\rm w}$ (g/mol)	$R_{\rm h}$ (nm)	$\frac{2R_{\rm h}}{d^a}$	$\frac{2R_{\rm h}}{d^{\rm b}}$	$\frac{2R_{\rm h}}{d^c}$
2-arm-PEG	2	10000	3.19 ± 0.15	3.19	2.13	1.28
4-arm-PEG	4	20000	3.95 ± 0.14	3.95	2.63	1.58
6-arm-PEG	6	30000	4.58 ± 0.14	4.58	3.05	1.83
8-arm-PEG	8	40000	5.14 ± 0.18	5.14	3.43	2.06

 $^{^{}a}d = 2 \text{ nm. }^{b}d = 3 \text{ nm. }^{c}d = 5 \text{ nm.}$

Characterization of PEGs. Dynamic light scattering (DLS) experiments were performed to determine the hydrodynamic radii (R_b) of the multiarm PEGs. DLS measurements were carried out using an ALV/CGS-3 compact goniometer (Langen, Germany) equipped with a solid-state laser light source (Cobalt Flamenco 100) emitting light at a wavelength λ of 660 nm with a power of 105 mW. The PEG samples were prepared at a concentration of 2 g/L for the DLS experiments. The scattered intensity-intensity correlation function with various delay times was measured at the temperature of 22 °C, with the scattering angle θ ranging from 30° to 90°. Using the CONTIN fitting procedure of data analysis of the intensityintensity correlation function as a function of the scattering wave vector $q = (4\pi/\lambda) \sin(\theta/2)$, the correlation function was found to exponentially decay with the delay time (Figure 2b). After finding that the decay rate was quadratic in q, the diffusion coefficient D was determined as shown in Figure 2c. Using the Stokes-Einstein relation for D and taking the viscosity of the solution as that of water (0.95 mPa.s), the hydrodynamic radius of the PEG molecule was obtained. Since prior research has shown that higher KCl concentrations in the medium enable enhanced detection of PEG translocation through nanopores, we have used 4 M KCl solution in our light scattering measurements. The experimentally determined values of R_h for the four multiarm PEGs are included in Table 1.

Nanopore Fabrication. We fabricated nanopores of desired diameter using controlled dielectric breakdown (CDB) of a thin lowstress silicon nitride membrane on a Si wafer. The membrane chips had a thickness of 10 nm and were customized from Norcada, Canada. The CDB process is described in previous publication.²⁵ Briefly, a DC voltage (less than 10 V) was applied across the membrane chip immersed in a fabrication buffer (1 M KCl, 10 mM HEPES, pH 8.0). While waiting in this fabrication step, there was a sudden increase in the detected ionic current through the membrane chip, signaling the breakdown of the membrane chip. The resulting pores were then conditioned with a conditioning buffer (3.6 M LiCl, 10 mM HEPES, pH 8.0) at a lower voltage (±2 V). During this conditioning stage, the conductance G of the pore was calculated from the I-V curve of the nanopore chip (shown in Figure 2d). The ohmic I-V curve indicates that the nanochannel is symmetrical, differing from the asymmetrical shape of protein nanopores like α -HL and Mycobacterium smegmatis porin A (MspA). The pore diameter d corresponding to the measured conductance was estimated using the following equation: 25,4

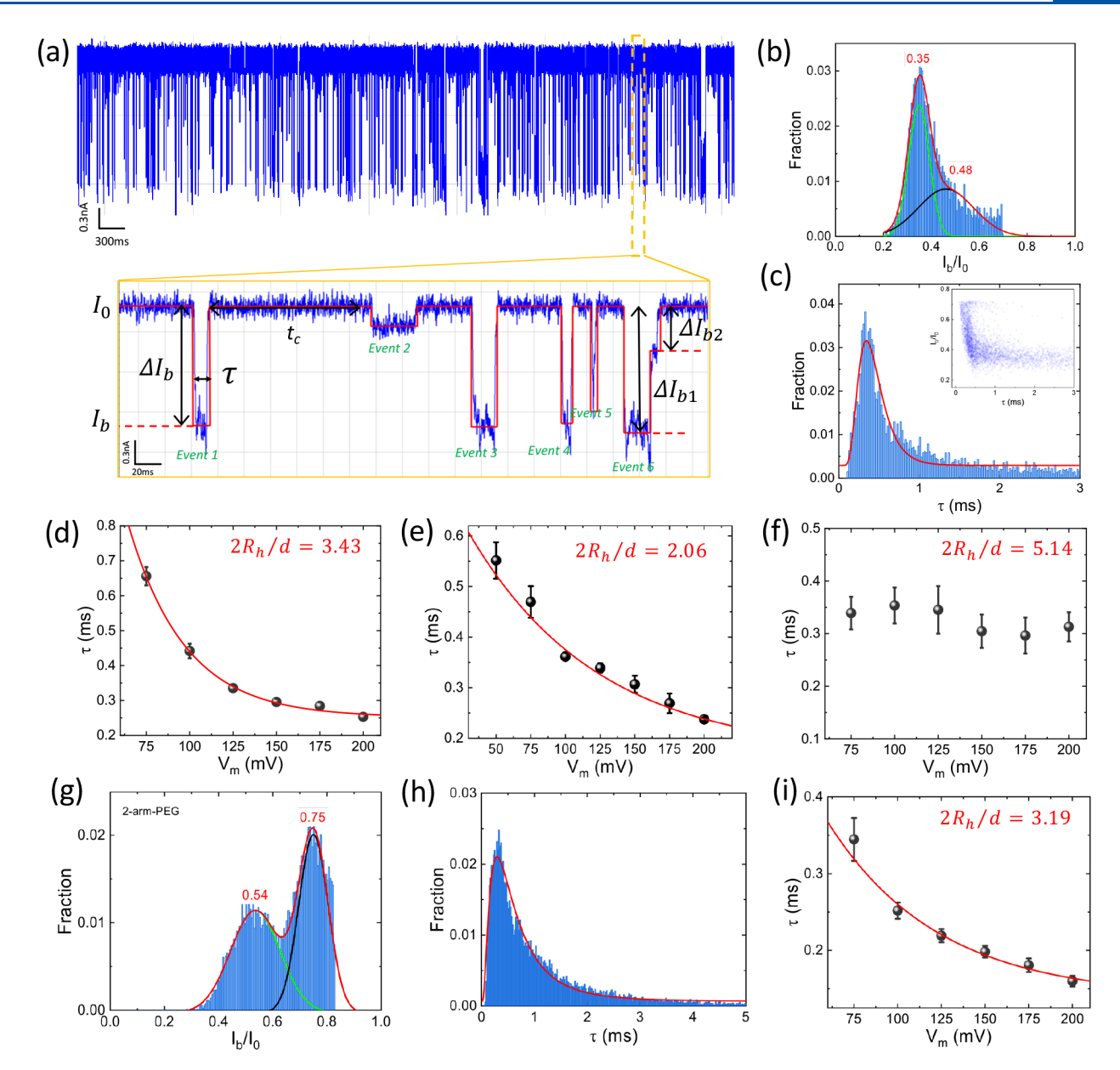


Figure 3. (a) A representative ionic current trace of 8-arm-PEG translocating through a 3 nm pore at 100 mV. The zoom-in shows a short period of the trace, which includes 6 translocation events. (b) Distribution of I_b/I_0 for 8-arm-PEG translocated in a 3 nm pore at 100 mV. More than 5000 events were used for statistical analysis. Solid lines represent Gaussian distribution fittings, and the peak positions are indicated. (c) Distribution of τ for 8-arm-PEG translocated in a 3 nm pore at 100 mV. The solid line represents the log-normal distribution fitting. The scatter plot of events is given in the inset. (d-f) The V_m dependence of τ for 8-arm-PEG translocated in nanopores of different $2R_h/d$, which are indicated in the figures. Solid lines represent exponential decay fittings. (g) Distribution of I_b/I_0 for 2-arm-PEG through 2 nm pore at 100 mV. (h) Distribution of τ for 2-arm-PEG through 2 nm pore at 100 mV. (i) V_m dependence of τ , with an exponential fitting.

$$d = \frac{G}{2\sigma} \left(1 + \sqrt{1 + \frac{16\sigma l}{\pi G}} \right) \tag{1}$$

where σ is the bulk solution conductivity, and l is the pore length. The conductivities of the fabrication buffer and conditioning buffer were 11.1 S/m and 16.3 S/m, respectively. The pore size was checked regularly during the conditioning stage until it reached the desired size. In the present study, our target pore diameters were d=2, 3, and 5 nm and the corresponding G values were 4.4 nS, 9.3 nS, and 22.9 nS, respectively, as obtained from the three I-V curves in Figure 2d. The values of d and the ratio $2R_{\rm h}/d$ (in the range of 1.3 to 5.1) are included in Table 1.

Translocation Experiments. The experimental setup for the single-molecule electrophoretic translocation through a single nanopore (as sketched in Figure 2e) consists of two chambers separated by

a thin membrane chip with a thickness of l. The only conductive pathway connecting these chambers is a nanopore with a diameter of d. By applying an external electric field across the membrane chip, PEG molecules in the donor chamber (cis-side) are forced to electrophoretically translocate through the nanopore toward the negative electrode connected to the acceptor chamber (trans-side). The translocation is associated with a free energy barrier emerging from the reduced entropy for localizing one end of the polymer chain at the entrance of the nanopore and the entropic barrier for squeezing the chain inside the pore. ¹⁶ The external electric field supplies the required energy for star-shaped polymers to surmount the free energy barrier and pass through the nanopore. During the translocation experiments, the concentration of PEG varied depending on the molecular weight, ranging from 0.01 g/L to 0.1 g/L. All measurements were conducted in an electrolyte solution containing 4 M KCl,

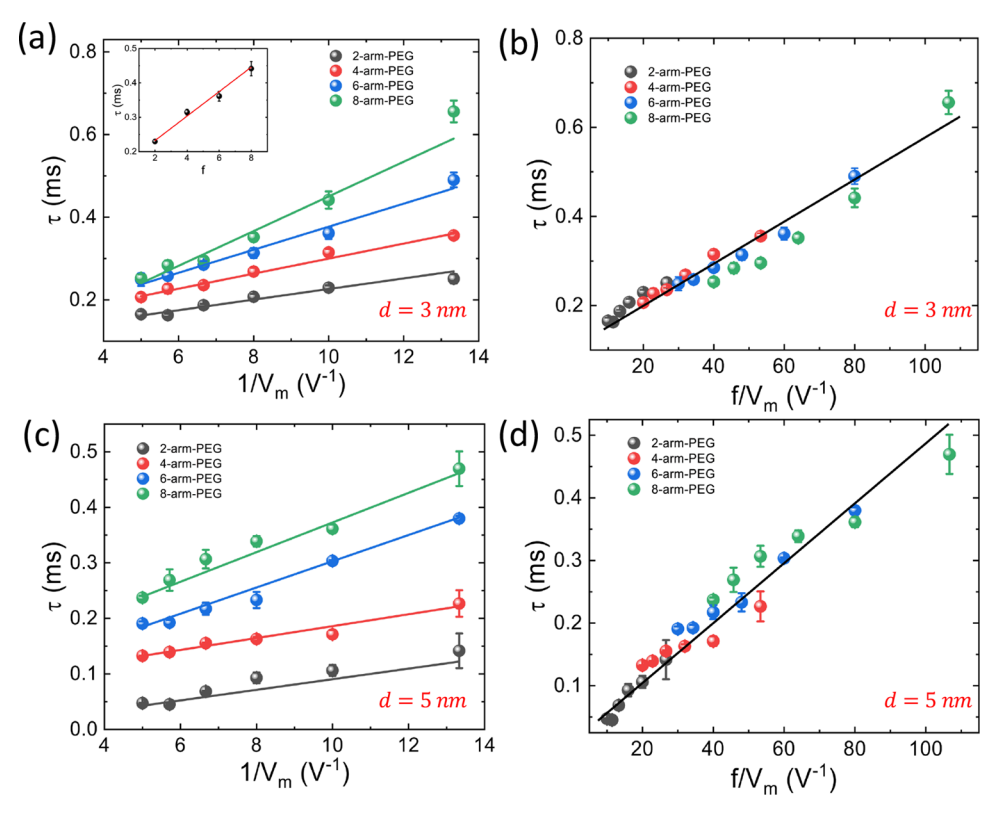


Figure 4. (a) The dwell time of multiarm-PEG translocation as a function of $1/V_{\rm m}$ in a 3 nm pore. The inset depicts the f dependence of τ at 100 mV. (b) The relationship between $f/V_{\rm m}$ and τ for multiarm-PEG translocation in a 3 nm pore. (c) The dwell time of multiarm-PEG translocation as a function of $1/V_{\rm m}$ in a 5 nm pore. (d) The relationship between $f/V_{\rm m}$ and τ for multiarm-PEG translocation in a 5 nm pore.

10 mM HEPES, and pH 6.0. The electric potential between the two chambers was controlled using silver/silver chloride (Ag/AgCl) electrodes connected to an Axopatch 200B patch clamp amplifier (Axon Instruments, CA). A Digidata 1550 data acquisition system and Axoscope software (Axon Instruments) were utilized to record the current trace with a 250 kHz acquisition rate and 10 kHz low-pass Bessel filter. The current traces were analyzed using MATLAB (The MathWorks, Inc., Natick, MA).

RESULTS AND DISCUSSION

Characteristics of Multiarm PEG Translocation. A representative example of the measured ionic current through a nanopore as a function of time is provided in Figure 3a. In this example, 8-arm-PEG molecules are electrophoretically driven through a 3 nm nanopore at 100 mV under the experimental conditions described in the experimental section. In the rendition at the top of Figure 3a, the recorded ionic current trace over a time duration of 4 s (from 4 to 8 s during the experiment) is shown. An expanded scale of the trace (covering the time range from 7.532 to 7.573 s) is provided at the bottom of Figure 3a. In this ionic current trace, the open pore current I₀ is 2.82 nA and it gets transiently blocked numerous times to a depressed ionic current I_b with a duration of time τ . We define the magnitude of the blocked current as $\Delta I_b = I_0 - I_b$. After each current blockage, the ionic current returns to the open pore current I_0 . The time taken for the next current blockage is t_c , denoting the time required to capture the next incoming molecule after the clearance of the previous molecules that encountered the nanopore.

The figure at the bottom of Figure 3a exhibits six typical events of polymer encounter across the nanopore. Focusing on the type "event 1", the magnitude of the blocked current

during this event is $\Delta I_b = I_0 - I_b$, and the dwell time of the polymer inside the nanopore is τ . The types of events 3–5 are analogous to the type of event 1. In contrast with these events, event 2 shows only a shallow blockage of current. As wellknown in single-molecule electrophoresis investigations through nanopores, such shallow blockages are attributed to collisions of the polymer at the pore entrance without successfully translocating into the trans chamber. Furthermore, some of the events exhibit a more complex behavior than event 1 and event 2 types, as seen in the event 6. In this event, there are two blockage levels, $\Delta I_{\rm b1}$ and $\Delta I_{\rm b2}$. Such features contain information on the conformation of the polymer during translocation. In the present situation of multiarm PEGs, translocation of star-shaped polymers in their asymmetric conformations $(f_{in} \neq f/2 \text{ can be discerned from such multiple-}$ state, but contiguous, blockage events. In the following discussion, we analyze only the deep blockage events and ignore the shallow blockage events (type event 2). However, we include all events in determining the capture rate.

The earmarks of the encounter of the polymer with the nanopore, namely, $I_{\rm b}$, $\Delta I_{\rm b}$, and τ , as well as the capture time $t_{\rm c}$ are highly stochastic. These observables are representations of the identity of the polymer (such as its chemical constitution, charge, size, shape, and conformations) and its interaction with the nanopore under the nonequilibrium condition of single-molecule electrophoresis. As a net result of all of these contributions to the translocation events, the values of $I_{\rm b}$ and τ are broadly distributed. The normalized distribution of the ratio of the blockage current to the open pore current, $(I_{\rm b}/I_{\rm o})$, is given in Figure 3b for 8-arm-PEG translocated through a 3 nm pore at 100 mV, where more than 5000 events are included. This histogram is fitted with two Gaussian curves

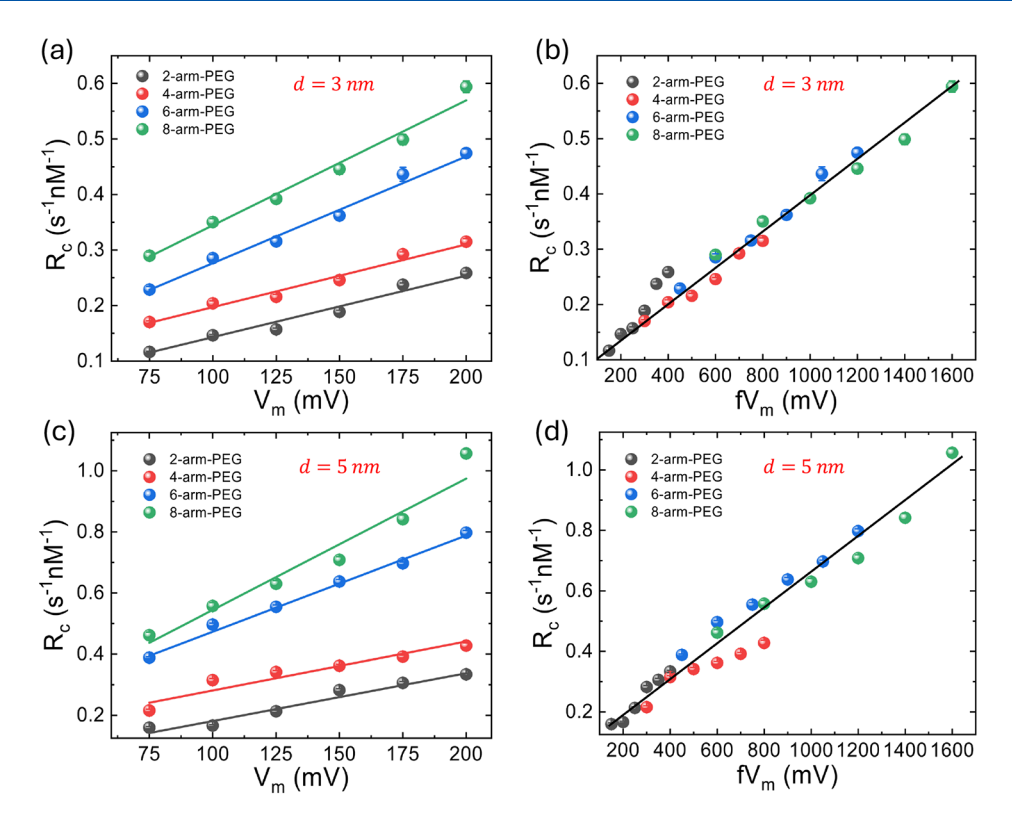


Figure 5. (a) $V_{\rm m}$ dependence of capture rate of multiarm-PEG in a 3 nm pore. (b) Capture rate of multiarm-PEG as a function of $fV_{\rm m}$ recorded in a 3 nm pore. (c) $V_{\rm m}$ dependence of capture rate of multiarm-PEG in a 5 nm pore. (d) Capture rate of multiarm-PEG as a function of $fV_{\rm m}$ recorded in a 5 nm pore. The solid lines in panels a and c represent linear fittings, whereas the lines in panels b and d serve as visual guides.

with peak positions at 0.35 (green curve corresponding to deeper blockage) and 0.48 (black curve corresponding to shallower blockage). The distribution corresponding to the green curve will be discussed below along with Figure 6. The normalized distribution of the dwell time τ for 8-arm-PEG translocating through a 3 nm pore at 100 mV is given in Figure 3c. The data from more than 5000 events are fitted with the log-normal distribution by following the standard practice in the previous works.²⁶ The peak position is taken as the characteristic translocation time τ . The scatter plot of events is shown in the inset of Figure 3c. The value of τ for the passage of the 8-arm-PEG through 3 nm nanopore at 100 mV is 0.44 ms (Figure 3c). Even though the time used in the histogram in Figure 3c is strictly dwell time, we attribute this time as the translocation time due to its monotonic decrease with an increase in the driving voltage as described next.

The dependence of the translocation time on the voltage (from 75 mV to 200 mV) for 8-arm-PEG through 3 nm pore $(2R_{\rm h}/d=3.43)$ is given in Figure 3d. The translocation time decreases exponentially with $V_{\rm m}$, which is a well-known characteristic of voltage dependence of successful translocation time. 10,15,19,20 When the experiments were repeated for a nanopore of 5 nm $(2R_h/d = 2.06)$, the dependence of τ on the voltage is given in Figure 3e. The same exponential dependence as in Figure 3d is seen, and now the translocation time is shorter due to the larger pore diameter. If the pore diameter is only 2 nm so that the polymer diameter is much bigger than the pore diameter $(2R_h/d = 5.14)$, the translocation of 8-arm-PEG through the nanopore is shut off. This is demonstrated in Figure 3f where the dwell time is independent of $V_{\rm m}$. On the other hand, the 2 nm pore can allow translocation if $2R_h$ is smaller. As an example, the

histograms of $I_{\rm b}/I_0$ and τ are given in Figure 3g and 3h, respectively, for the translocation of 2-arm-PEG through 2 nm pore at 100 mV ($2R_{\rm h}/d=2.43$). The data analysis of the histogram in Figure 3h (containing more than 10 000 events), as described above, gives the exponential dependence of τ on $V_{\rm m}$ (Figure 3i), corresponding to successful translocation events.

The results shown in Figure 3d—i clearly demonstrate that a small change in pore diameter can result in distinct characteristics of translocation events. More specifically, the significant difference between completely shutting down and fully opening the translocation through 2 nm pores for 8-arm-PEG and 2-arm-PEG, respectively, under identical experimental conditions exhibits the potential of electrophoretic translocation through nanopores for efficient separation and characterization of star-shaped polymers, where larger polymers are hindered from passing through smaller pores.

Dependence of Translocation Time on Number of Arms and V_m. In seeking to understand the role of the number of arms of f-arm-PEGs on the translocation time, we have investigated the single-molecule translocation of 2-arm, 4-arm, 6-arm, and 8-arm PEG molecules at different voltages. The results are given in Figure 4a for a 3 nm nanopore. Different colors on the data points denote different numbers of arms, as mentioned in the legend. The error bars (fitting error) are also shown for a few data points, and for the other data points, the error bars are smaller than the size of their symbol. As well-known in the literature, the average translocation time of uniformly charged linear polyelectrolytes through protein nanopores is proportional to $1/V_m$, in accordance with theoretical predictions for the experimental conditions where the drift from the electric field dominates the diffusion due to

thermal forces. 10,19 In view of this, we expect a linear relation between τ and $1/V_{\rm m}$ for each value of the number of arms (f) in the star polymer. Indeed, this expectation is found to be valid as seen in Figure 4a. While the data for $f=2,\,4,$ and 6 fall neatly on a straight line, there is one data point for the 8-arm-PEG at the lowest voltage studied (75 mV) that deviates from the straight line, indicating that for such a plot with such large value of f and low voltages, the translocation process is not fully in the drift-dominated regime.

Furthermore, for uniformly charged linear polyelectrolytes, the translocation time through a nanopore is proportional to the net charge Q of the polymer. 15,19 Since the arm length of the star-PEGs in the present study is uniform, the total charge of the star polymer is proportional to the number f of arms. Hence, analogous to the behavior of linear polymers, we expect the average translocation time of star polymers to be proportional to f. This expectation is found to be valid, as shown in the inset of Figure 4a, where τ is plotted against f for a 3 nm pore at 100 mV. Combining the dependencies of τ and Q and $V_{\rm m}$, the translocation time is expected to be linearly proportional to $Q/V_{\rm m}$, in the drift-dominated regime. By pooling together the data in Figure 4a for the various values of $V_{\rm m}$ and f, we plot τ versus $f/V_{\rm m}$ in Figure 4b. The error bars are also shown for a few data points, and for the other data points, the error bars are smaller than the size of their symbol. Figure 4b exhibits the universal behavior of linearity between τ and f/ $V_{\rm m}$ for multiarm-PEGs. The corresponding results for the pore diameter of 5 nm are given in Figure 4c and 4d.

Capture Rate. The primary step before a multiarm-PEG can translocate through a nanopore is that it must be captured at the entrance of the nanopore. Such capture events are indicated by the depressions in ionic current traces as time progresses, as shown in Figure 3a, independent of whether these depressions correspond to successful translocation events or simply collisions or failed translocation events. We define the capture rate R_c as the reciprocal of the product of the average of the time duration t_c between two successive events (defined in Figure 3a) and polymer concentration.

In general, the capture rate depends on three contributing factors: (a) diffusion, (b) pore-polymer interaction, and (c) electrophoretic drift in the cis chamber toward the pore entrance. 18 Furthermore, the capture rate is directly proportional to the pore diameter; namely, capture rate is higher if the pore diameter is larger. Since the applied potential gradient in the present experiments is considerably larger than the thermal energy (~25 mV for aqueous solutions at room temperature), the contribution from diffusion of the molecules to R_c can be safely ignored, in comparison with the electrophoretic contribution. Since the multiarm-PEGs studied here are relatively compact and hence their complexation interaction with the pore entrance is only meager, we anticipate that the electrophoretic drift will dominate the capture rate. The electrophoretic force resulting in polymer capture is the product of the total charge Q of the polymer and the applied electric field. Assuming a constant electric field across the pore (so that it is proportional to $V_{\rm m}$, we expect $R_{\rm c} \sim QV_{\rm m} \sim \bar{f}V_{\rm m}$. These expectations are borne out in our experiments.

The experimental results on the capture rate of f-arm-PEGs (f = 2, 4, 6, and 8) at the entrance of a 3 nm pore are given in Figure 5a as a function of $V_{\rm m}$. The capture rate is linear with $V_{\rm m}$, for each value of f. The slopes of the linear lines in Figure 5a are, of course, proportional to the net charge of the molecule. As evident in this figure, the slopes are increasing

progressively as f increases. In order to evaluate whether the slopes are linearly dependent on f, we present a master plot of $R_{\rm c}$ versus $fV_{\rm m}$ in Figure 5b, where the data in Figure 5a are used. We indeed observe a linear relation between $R_{\rm c}$ and $fV_{\rm m}$, consistent with the above theoretical argument. Thus, the capture rate is proportional to the molecular weight of the f-arm-PEG and the applied voltage.

The corresponding data for $R_{\rm c}$ when f-arm-PEGs (f = 2, 4, 6, and 8) are captured using a 5 nm nanopore are given in Figure 5c and 5d. The increase in pore diameter from 3 to 5 nm results in a substantial increase in the capture rate. For example, for the 8-arm-PEG captured at 100 mV, $R_{\rm c}$ increases to 0.55 s⁻¹ nM⁻¹ from 0.35 s⁻¹ nM⁻¹. The enhanced capture rate with a larger pore diameter is in agreement with the above theoretical argument.

The above results on $R_{\rm c}$, for both pore diameters, show that the capture rate is proportional to the molecular weight of the f-arm-PEG and the applied voltage. These results on PEG stars are in contrast with the molecular weight dependence of $R_{\rm c}$ of dsDNA at the nanopore entrance, where $R_{\rm c}$ was found to be independent of molecular weight in the drift-dominated regime. This difference is due to the fact that the multiarm-PEGs in the present study are compact and not stretched out like dsDNA in capillary electrophoresis experiments, so that the net charge is distributed inside the volume of the stars.

■ CONFORMATIONAL PARTITIONING DURING TRANSLOCATION

The blocked ionic current during the translocation event is a measure of the polymer conformation. As an example, we expect significant differences in the blocked current if the conformation of the star polymer undergoing translocation involves only one leading arm or multiple leading arms. Thus single-molecule electrophoresis of multiarm-PEG through a nanopore can reveal details of conformations of the stars as they traverse through the nanopore. In terms of viability of this approach to understand the mechanism of translocation of stars, there is precedence in the translocation of dsDNA through solid-state nanopores. In the experiments with dsDNA, the extent of the blocked current $\Delta I_b/I_0$ remained essentially constant with changes in the number of base pairs, 15,35 suggesting that single-arm or multiple-arm conformations can be detected in our experiments. Furthermore, in dsDNA translocation experiments using solid-state nanopores, two peaks are observed in the distribution of I_b/I_0 corresponding to one shallow blockage and one deep blockage. After considerable scrutiny of the data, the shallow and deep blockages have been assigned to single-file and folded conformations, respectively, during the passage of dsDNA through the nanopore.

Buttressed by such experimental observations on linear polyelectrolytes, we have monitored the details of the ionic current traces while translocation events are occurring. As a typical example, the distributions of $I_{\rm b}/I_0$ for multiarm-PEGs (f=2,4,6, and 8) passing through 3 nm nanopore at 100 mV are given in Figure 6 where the normalized fraction of events with a particular value of $I_{\rm b}/I_0$ (bin size is 0.005) is plotted against $I_{\rm b}/I_0$. Even with a cursory inspection, the distribution functions display significant differences between different values of f. In general, we have fitted the distribution functions using two Gaussians. For the 2-arm-PEG (Figure 6a), the peak positions for the shallow blockage ($I_{\rm b,s}/I_0$) and deep blockage ($I_{\rm b,d}/I_0$) are 0.9 and 0.84, respectively. These correspond to 0.1 and

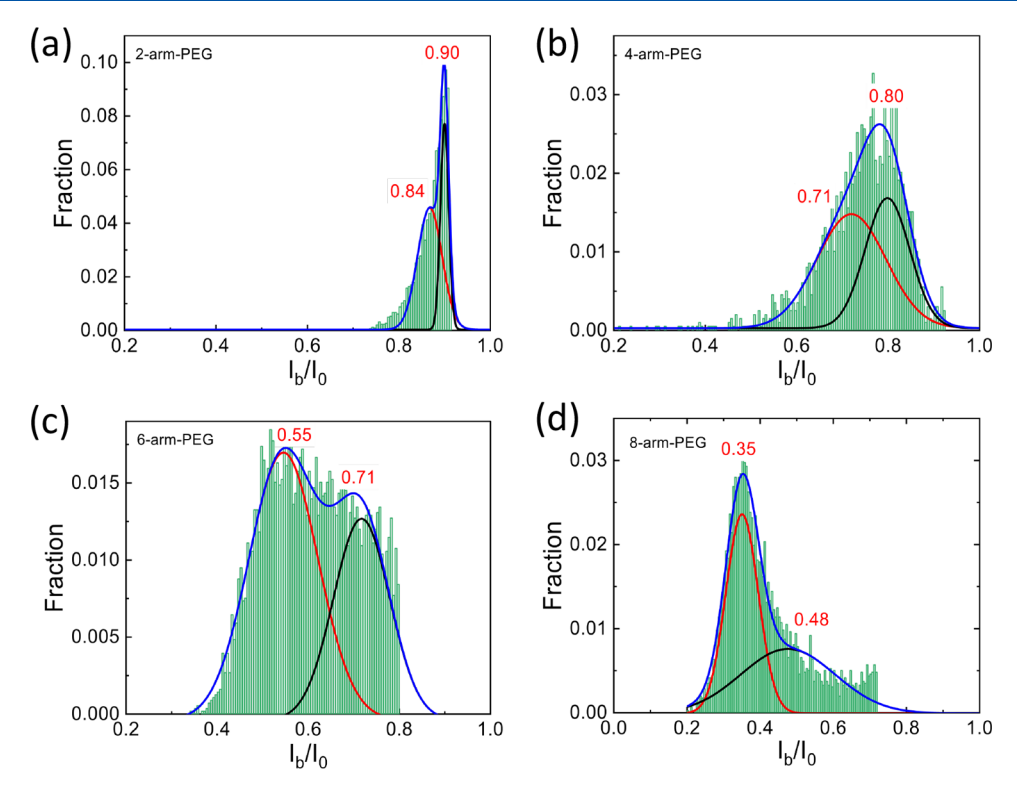


Figure 6. Distributions of I_b/I_0 for the translocation of multiarm-PEGs through a 3 nm pore at 100 mV: (a) 2-arm-PEG, (b) 4-arm-PEG, (c) 6-arm-PEG, and (d) 8-arm-PEG. The solid lines represent Gaussian distribution fittings with indicated peak positions.

0.16 for $\Delta I_{\rm b,s}$ and $\Delta I_{\rm b,d}$, respectively. We attribute these two blockage levels of 2-arm-PEG to linear conformations (shallow blockage) and folded conformations (deep blockage), analogous to the case of dsDNA. The observed ratio $\Delta I_{\rm b,d}/\Delta I_{\rm b,s}$ for the linear PEG is 1.6, whereas the corresponding value for dsDNA is ~2.0. This difference between linear PEG and dsDNA is in line with our expectation from the fact that PEG is more flexible than dsDNA.

As seen in Figure 6, the shallow blockages dominate for 2-arm-PEG and 4-arm-PEG, whereas deep blockages dominate for 6-arm-PEG and 8-arm-PEG. The distributions become wider as the number of arms increases. These variations clearly reveal the significant role played by the confinement parameter $2R_{\rm h}/d$ which transitions from 2.1 and 2.6 to 3.1 and 3.4, respectively for f=2 and 4, and f=6 and 8.

In addition to the differing weights of the shallow and deep blockages, the values of $I_{\rm b}/I_{\rm 0}$ at the peak of their respective distributions progressively decease (meaning more current blockage) as f increases. For, f=2, 4, 6, and 8, the corresponding peak values of $I_{\rm b}/I_{\rm 0}$ for shallow blockages are 0.90, 0.80, 0.71, and 0.48, respectively. The corresponding peak values of $I_{\rm b}/I_{\rm 0}$ for deep blockages are 0.84, 0.71, 0.55, and 0.35, respectively. The dependence of these peak values on f is summarized in Figure 7a, where the extent of the current blockage at the peak values, $\Delta I_{\rm b,peak}/I_{\rm 0}$ is plotted against f (red circles for shallow blockages and blue circles for deep blockages). As pointed out above, $\Delta I_{\rm b,peak}/I_{\rm 0}$ increases with f.

In order to estimate the number of forward arms $(f_{\rm in})$ and lagging arms $(f_{\rm out})$ of these star-shaped PEGs during translocation, we have used data on single-file 2-arm-PEG as a reference. Using this reference system, the data in Figure 7a are plotted in Figure 7b as the f-dependence of the normalized $\Delta I_{\rm b,peak}/I_0$. For example, in the case of 4-arm-PEG, $\Delta I_{\rm b,s}/I_0$ and $\Delta I_{\rm b,d}/I_0$ are 0.2 and 0.29, corresponding to 2 times and 3 times

 $\Delta I_{\rm b,s}/I_0$ of 2-arm-PEG, respectively. Thus, the shallow blockage in the translocation of 4-arm-PEG is attributed to its passage through the nanopore in a symmetrical shape ($f_{in} = f_{out} = 2$), as schematically illustrated in Figure 7c. Similarly, the deep blockage is associated with the asymmetrical shape of 4-arm-PEG during translocation, in a "1 + 3" or "3 + 1" manner, where the first number represents f_{in} and the second one is f_{out} . To normalize both $\Delta I_{\mathrm{b,s}}/I_0$ and $\Delta I_{\mathrm{b,d}}/I_0$ of other star-shaped PEGs, the $\Delta I_{b,s}/I_0$ of 2-arm-PEG is used as a benchmark, defining it as the normalized $\Delta I_{b,peak}/I_0$ as shown in Figure 7b. This normalized $\Delta I_{\rm b,peak}/I_0$ represents the number of single-file PEG arms when they occupy the nanopore, as illustrated in the schematic diagrams in Figure 7c. These diagrams depict four different situations of 4-arm-PEG passing through the nanopore, corresponding to $f_{\rm in}$ = 1, 2, 3, 4, respectively. In our analysis, we take the deepest current blockage in a single translocation event as Ib, regardless of the number of subblockages that constitute that blockage event. This approach gives the highest count of arms present within the nanopore during translocation, irrespective of whether they belong to $f_{\rm in}$ or f_{out} . This is why the translocation events of 4-arm-PEG in the "1 + 3" and "3 + 1" manners yield the same $\Delta I_b/I_0$, as shown in the schematic ionic current blockages in Figure 7c.

The four different scenarios depicted in Figure 7c can be classified into two types based on the number of stages: events containing one step or two steps. The two-step events can be further categorized into the first and third scenarios, depending on when the deeper blockage will appear. In this study, events are primarily classified based on three types of deep blockages: single-stage, double-stage, and multiple-stage, where the detection threshold is set at five times the standard deviation (STD)-baseline. Peaks with intervals exceeding 0.8 ms are classified as separate events. Each event may feature additional minor peaks besides the deepest current peak. If the absolute

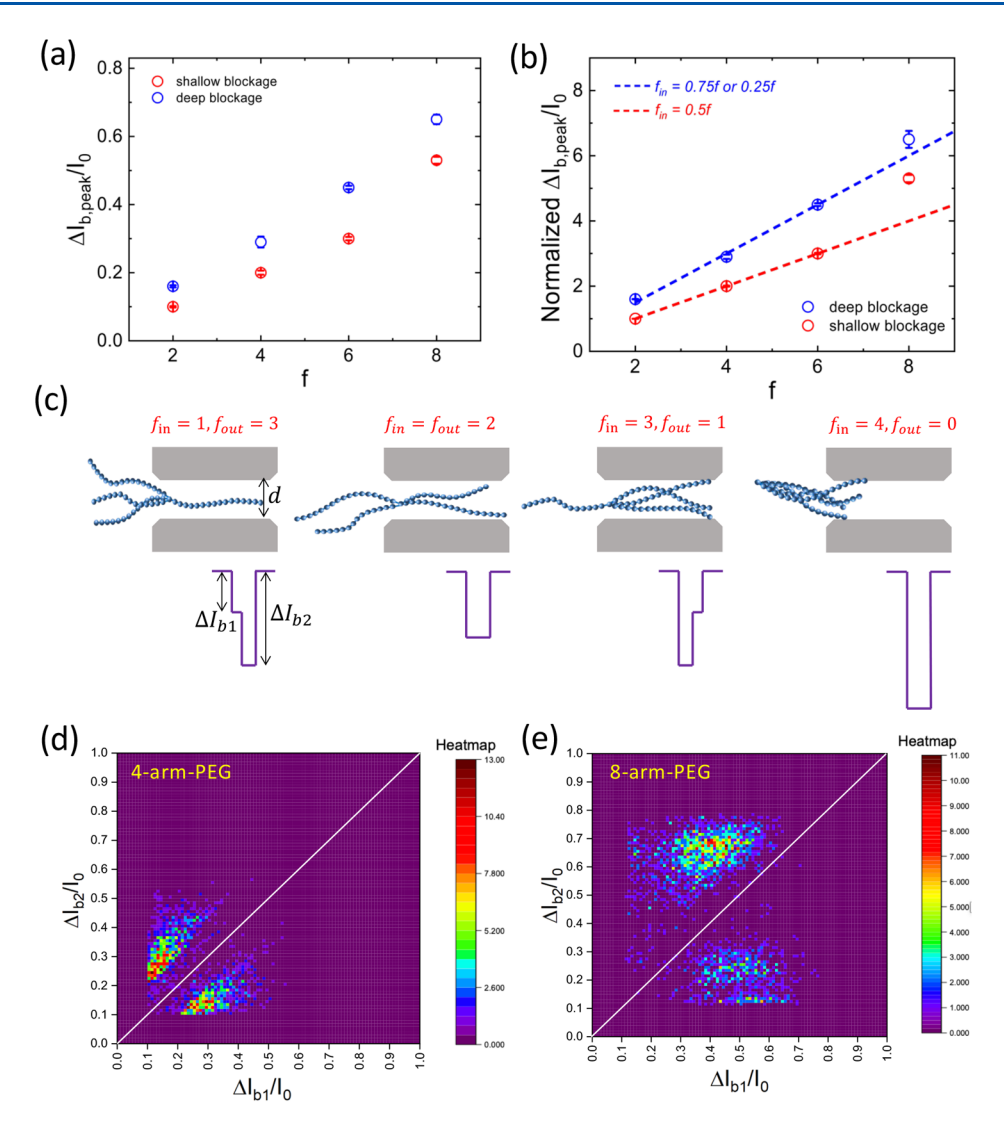


Figure 7. (a) The f dependence of $\Delta I_{\rm b,peak}/I_0$ for two sets of translocation events. (b) The f dependence of normalized $\Delta I_{\rm b,peak}/I_0$ for two sets of translocation events. d is 3 nm, and $V_{\rm m}$ is 100 mV. (c) Schematics illustrating the translocation of 4-arm-PEG in the nanopore with different $f_{\rm in}$ and the resulting ionic current blockages. (d) Heatmap displaying translocation events with two sub-blockage levels for 4-arm-PEG translocated through a 3 nm pore at 100 mV. (e) Same as (d) for 8-arm-PEG. I_0 , $I_{\rm b1}$, $I_{\rm b2}$, $\Delta I_{\rm b1}$, and $\Delta I_{\rm b2}$ are defined in the representative events shown in Figure 3a.

difference between these minor peaks and the deepest current peak is less than five times the STD-baseline, the event is classified as a single-stage event. If a minor peak's value differs from the deepest current value by more than five times the STD-baseline, and no other peaks deviate from this by more than five times the STD-baseline, the event is defined as a double-stage event. All other multipeak scenarios are classified as multiple-stage events, which are not further discussed in this study for simplification. The criterion of five times the STD-baseline is an optimized parameter.

As noted in Introduction, computer simulations suggested that translocation events with $f_{\rm in} > f_{\rm out}$ often result in unsuccessful translocation. ²⁹ In order to put our experimental results in this context, we have analyzed the difference between $\Delta I_{\rm b1}$ and $\Delta I_{\rm b2}$ in single translocation events featuring two subblockages (as illustrated in event 6 in Figure 3a). If the starshaped PEG passes through the nanopore with $f_{\rm in} > f_{\rm out}$ the first sub-blockage caused by the entrance of forward arms will be deeper than that of the following lagging arms, resulting in $\Delta I_{\rm b1} > \Delta I_{\rm b2}$. Conversely, if $f_{\rm in} < f_{\rm out}$ $\Delta I_{\rm b1}$ will be smaller than

 $\Delta I_{\rm b2}$. The heatmap (event diagram) of $\Delta I_{\rm b}$ for the translocation of 4-arm-PEG in an asymmetrical shape is displayed in Figure 7d, with the solid line denoting $\Delta I_{b1} = \Delta I_{b2}$ as a visual guide. From Figure 7d, it is evident that translocation events can be categorized into two groups based on the difference between the two sub-blockages: $\Delta I_{b1} < \Delta I_{b2}$ and $\Delta I_{b1} > \Delta I_{b2}$. The event diagram reveals that some of 4-arm-PEG chains can still successfully pass through the nanopore in the " $f_{\rm in} > f_{\rm out}$ " manner, entering the trans-side. While the 4-arm-PEG translocation frequently occurs in the manner of $\Delta I_{b1} > \Delta I_{b2}$, the majority of 8-arm-PEG translocations occur in the " $f_{\rm in}$ < f_{out} " manner, as shown in Figure 7e, suggesting that the optimal $f_{\rm in}$ is less than or equal to 0.5f. The two reference lines in Figure 7b correspond to $f_{in} = 0.25f$, 0.5f, respectively, covering all scenarios regarding $f_{\rm in}$ discussed in the previous studies on translocation of star-shaped polymers. We did not find any evidence for f_{in} = 4. We find that the shallow blockages in the translocation of 4-arm-PEG and 6-arm-PEG are close to 0.5f, indicating the symmetrical shape of these polymer chains during translocation. On the other hand, the shallow blockage

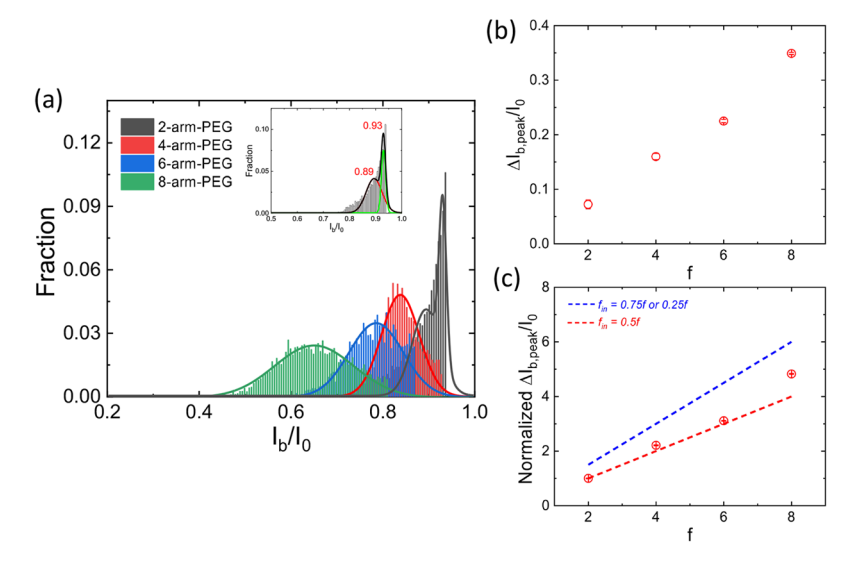


Figure 8. (a) Distributions of $I_{\rm b}/I_0$ for the translocation of multiarm-PEGs through a 5 nm pore at 100 mV. Gaussian distribution fittings are shown as solid lines. Inset is a zoom-in of the distribution of $I_{\rm b}/I_0$ for 2-arm-PEG. (b) f dependence of $\Delta I_{\rm b,peak}/I_0$ converted from the data in panel a. (c) f dependence of the normalized $\Delta I_{\rm b,peak}/I_0$.

of 8-arm-PEG deviates from 0.5f and is closer to 0.25f. Interestingly, all deep blockages align with the guideline of 0.25f. As mentioned above, besides the finding that the optimal $f_{\rm in}$ is 0.5f in previous flow-induced translocation experiments, ²² the simulation study has demonstrated that the optimal $f_{\rm in}$ will change from 0.5f to 0.25f as the degree of confinement increases. ²⁸ In qualitative agreement with these simulation results on flow-induced translocation of uncharged stars, we find that, for charged stars undergoing electrophoretic translocation, the optimal $f_{\rm in}$ will shift from 0.5f to 0.25f as the degree of confinement increases. Moreover, the results in Figure 6 also show that with the increase of f, deep blockage becomes dominant, and this deep blockage corresponds precisely to the case where $f_{\rm in}$ equals 0.25f as shown by the blue line in Figure 7b.

Confinement Effect. We have already shown in Figure 6 that the confinement parameter $2R_h/d$ plays a significant role in dictating the distribution functions of blocked currents, both shallow and deep. Since the pore diameter for the data in Figure 6 is 3 nm, which is quite tight for the passage of multiarm-PEGs, the distribution functions corresponding to the shallow and deep blockages overlapped significantly. In order to further investigate the role of confinement on the features of translocation of multiarm-PEGs, we have studied a 5 nm nanopore, where the confinement is less severe in comparison with the case of Figure 6. We did not choose larger pores because the extent of current blockage is a smaller fraction of open pore current, and the translocation time is faster, pushing the detection limit of the instrumentation, both reducing the signal-to-noise ratio. The distribution functions of $I_{\rm h}/I_0$ for the f-arm-PEGs (f = 2, 4, 6, and 8) are displayed in Figure 8. While two peaks are still evident in the blockage current ratio distribution for linear PEG, only a single peak is observed for the other three multiarm PEGs. In 3 nm pores, the two peaks for linear PEG were attributed to single-file and folded configurations of the polymer chain during translocation. However, in 5 nm pores, a single, narrow peak in the distribution for multiarm PEGs, replaces the broad distribution seen in 3 nm pores. Figure 8b and 8c presents the fdependence of $\Delta I_{b,peak}/I_0$ and the normalized $\Delta I_{b,peak}/I_0$ on f,

respectively. In this scenario, all data points tend to align with the guideline of $f_{\rm in}=0.5f$, contrasting with the behavior observed in 3 nm pores (Figure 7). This finding supports the notion that as the pore size increases and the degree of confinement decreases, the optimal $f_{\rm in}$ shifts from 0.25f to 0.5f.

CONCLUSIONS

We have experimentally studied the conformational trajectories of star-like polymers when they are squeezed through a single nanopore of dimensions comparable to those of the polymer. Capitalizing on the behavior of polyethylene glycol (PEG) in KCl solutions as polycations, we have investigated several well-characterized multiarm-PEG molecules using single-molecule electrophoresis through a single nanopore. In the present study, we have varied the number (f) of arms of the star-polymers and kept the arm length the same so that the exclusive role of f on the characteristics of their translocation through a narrow pore can be evaluated.

One of our key findings is the direct inference of conformational modes of translocation of star-like polymers. As an example, the translocation of 4-arm-PEG through a 3 nm nanopore exhibits conformational partitioning involving two distinct modes. In one mode of translocation, the chain conformation inside the nanopore is symmetric where the fraction of the number of arms $f_{\rm in}$ in the forward direction is 1/2. In the other mode of translocation, $f_{\rm in}$ is f/4. Depending on the extent of confinement of the star-polymer inside the nanopore, $f_{\rm in}$ is in the range between f/2 and f/4. We have also observed $f_{\rm in} > f/2$.

In general, we find the average translocation time τ to be proportional to the ratio of the number of arms (f) and the applied voltage gradient $(V_{\rm m})$, $\tau \sim f/V_{\rm m}$. Since the arm length of the stars is kept constant, this result is equivalent to $\tau \sim Q/V_{\rm m} \sim M/V_{\rm m}$, where Q and M are, respectively, the total charge and molar mass of the polymer. This observation is consistent with the universal behavior of translocation time for uniformly charged linear polyelectrolytes in the drift-dominated regime appearing for strong enough voltage gradients. On the other hand, the capture rate $R_{\rm c}$ is found to be proportional to the product of f and $V_{\rm m}$, $R_{\rm c} \sim fV_{\rm m}$. Since the arm length is fixed,

this result is equivalent to $R_{\rm c} \sim MV_{\rm m}$, which is different from the corresponding result in the drift-dominated regime for linear polyelectrolytes where $R_{\rm c}$ is independent of molar mass of the translocating polymer. We attribute this difference to the compact three-dimensional nature of the star-polymer in contrast to the one-dimensional conformation of linear polymers during translocation process.

In addition to characterizing the fundamental processes of translocation of star-polymers, we find that the nanopores are selective in terms their allowance of translocation of different numbers of arms in multiarm-PEGs. As an example, 2 nm nanopores do not allow passage of 8-arm-PEGs while 2-arm-PEGs easily pass through.

There are several immediate future steps in extending the present study and fine-tuning the characterization and selectivity of star-polymers. As an example, the roles of different arm lengths, surface-modification of the nanopore, and gradients in ionic strength and pH of the medium are of great interest. In general, the single-molecule electrophoresis method implemented here has great potential in characterization and selective separation of all branched polymers, such as stars, combs, and brushes, in aqueous media.

AUTHOR INFORMATION

Corresponding Author

Murugappan Muthukumar — Department of Polymer Science and Engineering, University of Massachusetts, Amherst, Massachusetts 01003, United States; oorcid.org/0000-0001-7872-4883; Email: muthu@umass.edu

Authors

Kuo Chen — Department of Polymer Science and Engineering, University of Massachusetts, Amherst, Massachusetts 01003, United States; Oorcid.org/0000-0002-0459-4139

Minglun Li − Department of Polymer Science and Engineering, University of Massachusetts, Amherst, Massachusetts 01003, United States; orcid.org/0000-0002-1286-6915

Complete contact information is available at: https://pubs.acs.org/10.1021/acs.macromol.4c01092

Notes

The authors declare no competing financial interest.

ACKNOWLEDGMENTS

We thank the National Science Foundation (grant no. DMR 2309539) and AFOSR (grant no. FA9550-23-1-0584) for financial support.

REFERENCES

- (1) Muthukumar, M. Mechanism of DNA Transport Through Pores. *Annu. Rev. Biophys. Biomol. Struct.* **2007**, *36*, 435–450.
- (2) Branton, D.; Deamer, D. W.; Marziali, A.; Bayley, H.; Benner, S. A.; Butler, T.; Di Ventra, M.; Garaj, S.; Hibbs, A.; Huang, X.; et al. The Potential and Challenges of Nanopore Sequencing. *Nat. Biotechnol.* **2008**, *26*, 1146–1153.
- (3) Bergsbaken, T.; Fink, S. L.; Cookson, B. T. Pyroptosis: Host Cell Death and Inflammation. *Nat. Rev. Microbiol.* **2009**, *7*, 99–109.
- (4) Saxena, A.; Tripathi, B. P.; Kumar, M.; Shahi, V. K. Membrane-Based Techniques for the Separation and Purification of Proteins: An Overview. *Adv. Colloid Interface Sci.* **2009**, *145*, 1–22.
- (5) Strambio-De-Castillia, C.; Niepel, M.; Rout, M. P. The Nuclear Pore Complex: Bridging Nuclear Transport and Gene Regulation. *Nat. Rev. Mol. Cell Biol.* **2010**, *11*, 490–501.

- (6) Yang, N. J.; Hinner, M. J. Getting Across the Cell Membrane: An Overview for Small Molecules, Peptides, and Proteins. *Site-Specific Protein Labeling: Methods and Protocols* **2015**, 1266, 29–53.
- (7) De Gennes, P.-G. Coil-Stretch Transition of Dilute Flexible Polymers Under Ultrahigh Velocity Gradients. *J. Chem. Phys.* **1974**, *60*, 5030–5042.
- (8) De Gennes, P.-G. Reptation of Stars. J. Phys. (Paris) 1975, 36, 1199-1203.
- (9) Klein, J.; Fletcher, D.; Fetters, L. J. Dynamics of Entangled Star-Branched Polymers. *Faraday Symp. Chem. Soc.* **1983**, *18*, 159–171.
- (10) Kasianowicz, J. J.; Brandin, E.; Branton, D.; Deamer, D. W. Characterization of Individual Polynucleotide Molecules Using a Membrane Channel. *Proc. Natl. Acad. Sci. U. S. A.* **1996**, 93, 13770—13773.
- (11) Bezrukov, S. M.; Vodyanoy, I.; Brutyan, R. A.; Kasianowicz, J. J. Dynamics and Free Energy of Polymers Partitioning into a Nanoscale Pore. *Macromolecules* **1996**, 29, 8517–8522.
- (12) Meller, A.; Nivon, L.; Branton, D. Voltage-Driven DNA Translocations Through a Nanopore. *Phys. Rev. Lett.* **2001**, *86*, 3435.
- (13) Jin, F.; Wu, C. Observation of the First-Order Transition in Ultrafiltration of Flexible Linear Polymer Chains. *Phys. Rev. Lett.* **2006**, *96*, 237801.
- (14) Rodrigues, C. G.; Machado, D. C.; Chevtchenko, S. F.; Krasilnikov, O. V. Mechanism of KCl Enhancement in Detection of Nonionic Polymers by Nanopore Sensors. *Biophys. J.* **2008**, 95, 5186—5192.
- (15) Wanunu, M.; Sutin, J.; McNally, B.; Chow, A.; Meller, A. DNA Translocation Governed by Interactions with Solid-State Nanopores. *Biophys. J.* **2008**, *95*, 4716–4725.
- (16) Kumar, R.; Muthukumar, M. Origin of Translocation Barriers for Polyelectrolyte Chains. *J. Chem. Phys.* **2009**, *131*. DOI: 10.1063/1.3264632
- (17) Reiner, J. E.; Kasianowicz, J. J.; Nablo, B. J.; Robertson, J. W. Theory for Polymer Analysis Using Nanopore-Based Single-Molecule Mass Spectrometry. *Proc. Natl. Acad. Sci. U. S. A.* **2010**, *107*, 12080–12085
- (18) Muthukumar, M. Theory of Capture Rate in Polymer Translocation. J. Chem. Phys. 2010, 132. DOI: 10.1063/1.3429882
- (19) Wong, C. T. A.; Muthukumar, M. Polymer Translocation Through α -Hemolysin Pore with Tunable Polymer-Pore Electrostatic Interaction. *J. Chem. Phys.* **2010**, *133*, 07B607.
- (20) Chen, Q.; Liu, J.; Schibel, A. E.; White, H. S.; Wu, C. Translocation Dynamics of Poly (styrenesulfonic acid) Through an α -Hemolysin Protein Nanopore. *Macromolecules* **2010**, *43*, 10594–10599.
- (21) Wanunu, M.; Morrison, W.; Rabin, Y.; Grosberg, A. Y.; Meller, A. Electrostatic Focusing of Unlabelled DNA into Nanoscale Pores Using a Salt Gradient. *Nat. Nanotechnol.* **2010**, *5*, 160–165.
- (22) Ge, H.; Pispas, S.; Wu, C. How Does a Star Chain (Nanooctopus) Crawl Through a Nanopore? *Polymer Chem.* **2011**, 2, 1071–1076.
- (23) Li, L.; He, C.; He, W.; Wu, C. How Does a Hyperbranched Chain Pass Through a Nanopore? *Macromolecules* **2012**, *45*, 7583–7589
- (24) Breton, M. F.; Discala, F.; Bacri, L.; Foster, D.; Pelta, J.; Oukhaled, A. Exploration of Neutral Versus Polyelectrolyte Behavior of Poly (ethylene glycol) s in Alkali Ion Solutions Using Single-Nanopore Recording. *J. Phys. Chem. Lett.* **2013**, *4*, 2202–2208.
- (25) Kwok, H.; Briggs, K.; Tabard-Cossa, V. Nanopore Fabrication by Controlled Dielectric Breakdown. *PloS One* 2014, 9, No. e92880.
 (26) Jeon, B.-j.; Muthukumar, M. Determination of Molecular
- Weights in Polyelectrolyte Mixtures Using Polymer Translocation Through a Protein Nanopore. ACS Macro Lett. 2014, 3, 911–915.
- (27) Liu, Z.; Liu, J.; Xiao, M.; Wang, R.; Chen, Y.-L. Conformation-Dependent Translocation of a Star Polymer through a Nanochannel. *Biomicrofluidics* **2014**, *8*, 054107.
- (28) Ding, M.; Duan, X.; Shi, T. Flow-Induced Translocation of Star Polymers through a Nanopore. *Soft Matter* **2016**, *12*, 2851–2857.

- (29) Katkar, H.; Muthukumar, M. Single Molecule Electrophoresis of Star Polymers through Nanopores: Simulations. *J. Chem. Phys.* **2018**, *149*, 163306.
- (30) Karawdeniya, B. I.; Bandara, Y.; Nichols, J. W.; Chevalier, R. B.; Dwyer, J. R. Surveying Silicon Nitride Nanopores for Glycomics and Heparin Quality Assurance. *Nat. Commun.* **2018**, *9*, 1–8.
- (31) Karau, P.; Tabard-Cossa, V. Capture and Translocation Characteristics of Short Branched DNA Labels in Solid-State Nanopores. ACS Sens. 2018, 3, 1308–1315.
- (32) He, L.; Karau, P.; Tabard-Cossa, V. Fast Capture and Multiplexed Detection of Short Multi-Arm DNA Stars in Solid-State Nanopores. *Nanoscale* **2019**, *11*, 16342–16350.
- (33) Nagarajan, K.; Chen, S. B. Translocation of Star Polyelectrolytes through a Nanopore. *J. Phys. Chem. B* **2019**, *123*, 3124–3134.
- (34) Nagarajan, K.; Chen, S. B. Flow-Induced Translocation of Star Polymers through a Nanopore. *J. Phys. Chem. B* **2019**, 123, 7919–7925.
- (35) Brinkerhoff, H.; Kang, A. S.; Liu, J.; Aksimentiev, A.; Dekker, C. Multiple Rereads of Single Proteins at Single—Amino Acid Resolution Using Nanopores. *Science* **2021**, *374*, 1509—1513.
- (36) Yu, L.; Kang, X.; Li, F.; Mehrafrooz, B.; Makhamreh, A.; Fallahi, A.; Foster, J. C.; Aksimentiev, A.; Chen, M.; Wanunu, M. Unidirectional Single-File Transport of Full-Length Proteins Through a Nanopore. *Nat. Biotechnol.* **2023**, *41*, 1130.
- (37) Chen, K.; Muthukumar, M. Substantial Slowing of Electrophoretic Translocation of DNA through a Nanopore Using Coherent Multiple Entropic Traps. *ACS Nano* **2023**, *17*, 9197–9208.
- (38) Zhou, C.; Ji, C.; Nie, Y.; Yang, J.; Zhao, J. Poly (Ethylene Oxide) Is Positively Charged in Aqueous Solutions. *Gels* **2022**, *8*, 213.
- (39) Cao, N.; Zhao, Y.; Chen, H.; Huang, J.; Yu, M.; Bao, Y.; Wang, D.; Cui, S. Poly(Ethylene Glycol) Becomes a Supra-Polyelectrolyte by Capturing Hydronium Ions in Water. *Macromolecules* **2022**, *55*, 4656–4664.
- (40) Waugh, M.; Briggs, K.; Gunn, D.; Gibeault, M.; King, S.; Ingram, Q.; Jimenez, A. M.; Berryman, S.; Lomovtsev, D.; Andrzejewski, L.; et al. Solid-State Nanopore Fabrication by Automated Controlled Breakdown. *Nat. Protoc.* **2020**, *15*, 122–143.
- (41) Kowalczyk, S. W.; Grosberg, A. Y.; Rabin, Y.; Dekker, C. Modeling the Conductance and DNA Blockade of Solid-State Nanopores. *Nanotechnology* **2011**, 22, 315101.